AGU PUBLICATIONS

Geophysical Research Letters

RESEARCH LETTER
10.1002/2015GL064874

Key Points:
- High-speed imaging of gas-pyroclasts interaction in starting volcanic jets
- Velocity and deceleration profiles of pyroclasts in the jet are outlined
- A velocity-dependent reduced drag zone forms and trails behind the jet head

Correspondence to:
J. Taddeucci,
jacopo.taddeucci@ingv.it

Citation:
Taddeucci, J., M. A. Alatorre-Ibarguengoitia, D. M. Palladino, P. Scarlato, and C. Camaldo (2015), High-speed imaging of Strombolian eruptions: Gas-pyroclast dynamics in initial volcanic jets, *Geophys. Res. Lett.*, *42*, 6253–6260, doi:10.1002/2015GL064874.

Received 9 JUN 2015
Accepted 17 JUL 2015
Accepted article online 20 JUL 2015
Published online 4 AUG 2015

High-speed imaging of Strombolian eruptions: Gas-pyroclast dynamics in initial volcanic jets

J. Taddeucci[1], M. A. Alatorre-Ibarguengoitia[2], D. M. Palladino[3], P. Scarlato[1], and C. Camaldo[3]

[1]Istituto Nazionale di Geofisica e Vulcanologia, Rome, Italy, [2]Universidad de Ciencias y Artes de Chiapas, Tuxtla Gutiérrez, Mexico, [3]Dipartimento di Scienze della Terra, Sapienza Università di Roma, Rome, Italy

Abstract High-speed imaging of Strombolian explosions brings into view the motion of pyroclasts upon leaving the volcanic vent. The erupted gas-pyroclast mixtures form jets with well-defined leading vortex rings that rise at almost constant velocity proportional to the time-averaged velocity of pyroclasts. The ejection velocity of pyroclasts decreases over time and defines a conical profile centered on the jet central streamline. Pyroclast deceleration patterns are related to their velocity and compatible with drag force but are also strongly controlled by jet dynamics. These patterns include constant, decreasing, or abruptly increasing decelerations up to 10^4 m s^{-2}. Nonuniform deceleration focuses at the jet sides and, mostly, in a narrow zone across the vortex ring. This deceleration zone is trailed by a reduced drag zone, where deceleration is drastically reduced. In these highly transient eruptions, both zones move upward and attenuate over time. Our results provide the first quantitative mapping of reduced drag zones.

1. Introduction

Subaerial explosive volcanism injects a mixture of gas and volcanic fragments (pyroclasts) into the atmosphere. This fast-moving mixture undergoes a highly variable and complex series of processes that ultimately control the effects of the eruption on the surrounding environment. Here we use high-speed imaging to describe and parameterize the interactions of pyroclasts with volcanic gas and the surrounding atmosphere during the initial phase of volcanic jets from Strombolian-style explosive volcanic activity.

The dispersal of pyroclasts by explosive eruptions is controlled by their interactions with the volcanic gas in the eruptive mixture and the atmosphere. Volcanologists usually recognize two end-members in the degree of interaction, with (i) bomb and lapilli that decouple soon from the gas phase and follow mainly ballistic trajectories and (ii) fine lapilli and ash that remain coupled with the gas on eruption timescales. The devastation caused by volcanic bombs falling near the summit of Ontakesan volcano (Japan) in 2014 [*Global Volcanism Program*, 2015] and the international dispersion of ash by the ongoing (at the time of writing) eruption of the Chilean volcano Calbuco (SERNAGEOMIN RAV Región de Los Lagos Año 2015 Abril - Volumen 4, http://www.sernageomin.cl/reportesVolcanes/20150506070433816RAV_Los_Lagos_2015_05_04_vol_18_Abril.pdf) are the two most recent, dramatic examples of these end-members. Ballistic models have been proposed with the double aim of predicting the range of falling coarse pyroclasts and back-tracking eruption parameters from the pyroclast landing position. Most of these models assume that pyroclasts are ejected into still air upon leaving the vent, and therefore, their trajectory can be described as simply ballistic [e.g., *Wilson*, 1972; *Alatorre-Ibarguengoitia and Delgado-Granados*, 2006]. However, many authors have pointed out cases where the field distribution of pyroclasts cannot be explained by classic ballistic models, remarking that pyroclasts are not ejected into still air, yet they travel into an expanding gas volume, which significantly reduces the drag force near the vent [e.g., *Fagents and Wilson*, 1993; *Mastin*, 2001; *de' Michieli Vitturi et al.*, 2010; *Alatorre-Ibarguengoitia et al.*, 2012]. To date, the ground-truth validation of this fundamental process is stalled by the paucity of direct observation and measurement of gas-pyroclast coupling during an eruption.

Stromboli volcano (Italy) hosts persistent, relatively accessible explosive eruptive activity. The volcano summit area is a popular tourist destination, although subject to the hazard of occasional ballistic fallout from the active vents nearby. For decades, this area has also been used for volcano imaging studies. For instance, thermal infrared cameras have been used both to study the rise velocity of eruption plumes and to characterize explosion phases based on the coupling or decoupling of pyroclasts with the gas phase, also drawing inferences on the density of the gas phase [*Patrick*, 2007; *Harris et al.*, 2012; *Bombrun et al.*, 2015]. High-speed, visible light cameras are well suited for tracking individual pyroclasts, allowing one to relate their

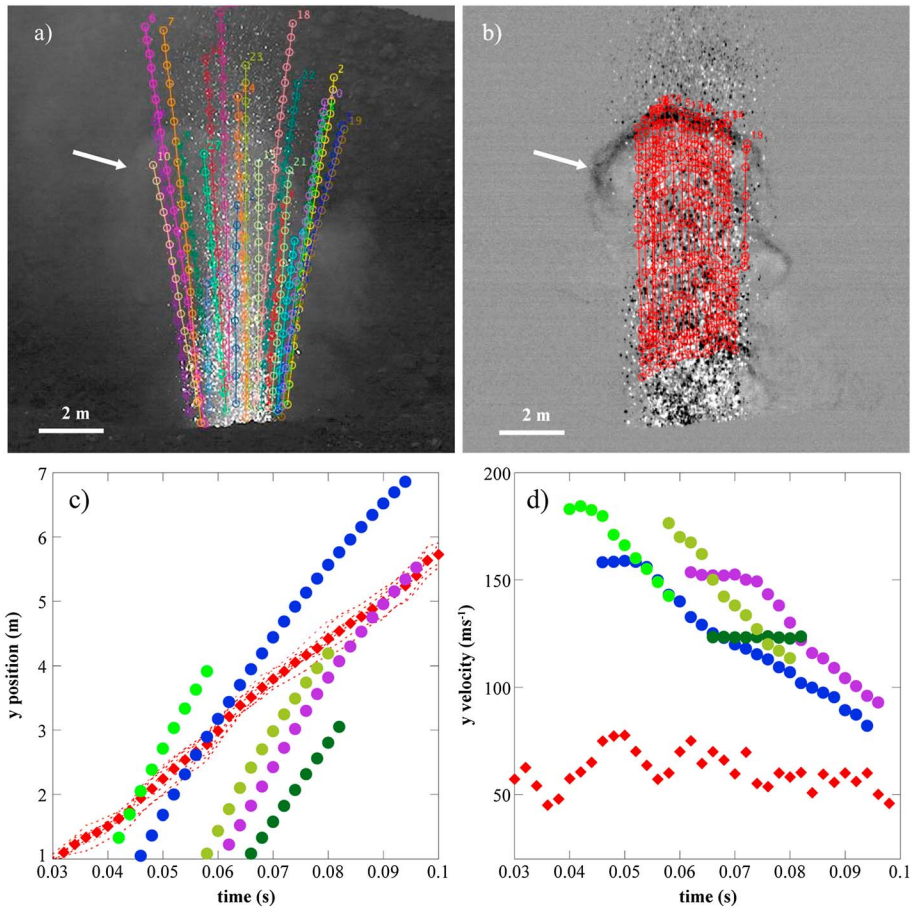

Figure 1. (a) Still frame of the initial jet from a Strombolian explosion. Pyroclasts (bright spots) travel within a (darker) gas cloud. Tracked pyroclast trajectories are shown in color. (b) Difference image of Figure 1a, highlighting the gas in and around the jet and the leading vortex ring (white arrow), whose front was also tracked (in red). (c) Vertical position over time for five representative tracked pyroclasts (colored dots) and the leading vortex front (red dashed lines; red diamonds is their average). (d) Vertical velocity of the same pyroclasts and leading vortex front over time.

ejection velocity, size, and angle to the dynamics and energetics of pressure release in the volcanic conduit [*Gaudin et al.*, 2014]. Here we take advantage of the high spatial and temporal resolution of high-speed, visible light cameras to provide new qualitative and quantitative insights on how centimeter-sized pyroclasts interact with volcanic and atmospheric gases in the initial phase of volcanic jets.

2. Tracking Pyroclasts in Initial Jets

Here we focus on five Strombolian explosions that occurred at the north-east vent area of Stromboli volcano between 11:04:46 and 13:32:04 GMT (Greenwich Mean Time) on 19 June 2009. We filmed the explosive activity at 500 frames per second using a NAC HotShot 512 SC monochrome high-speed camera with 512×512 pixels, providing, with a 300 mm focal length lens at a distance of 326 ± 10 m from the vent, a resolution of 0.018 m/pixel and a field of view (hereafter FOV) of 8.9 m. Individual explosions, very similar to each other, featured the jet-like ejection of gas and pyroclasts (30–36 tons) over 10–15 s, and included multiple ejection pulses, the fastest pyroclasts being the first to leave the vent [*Gaudin et al.*, 2014]. The onset of each explosion is marked by the displacement of a dilute gas cloud previously hovering above the vent. Then, a jet of well-collimated, small (a few centimeters) pyroclasts exits the vent and immediately starts to develop a leading vortex ring—a torus-shaped vortex associated with the injection of a fluid into another one and a common occurrence in volcanic eruptions [e.g., *Kieffer and Sturtevant*, 1984].

Pyroclasts were manually tracked over the entire FOV using the MTrackJ plug-in of the freeware software ImageJ [*Abramoff et al.*, 2004]. We focus on the initial phase of the jet, when pyroclast velocity is highest

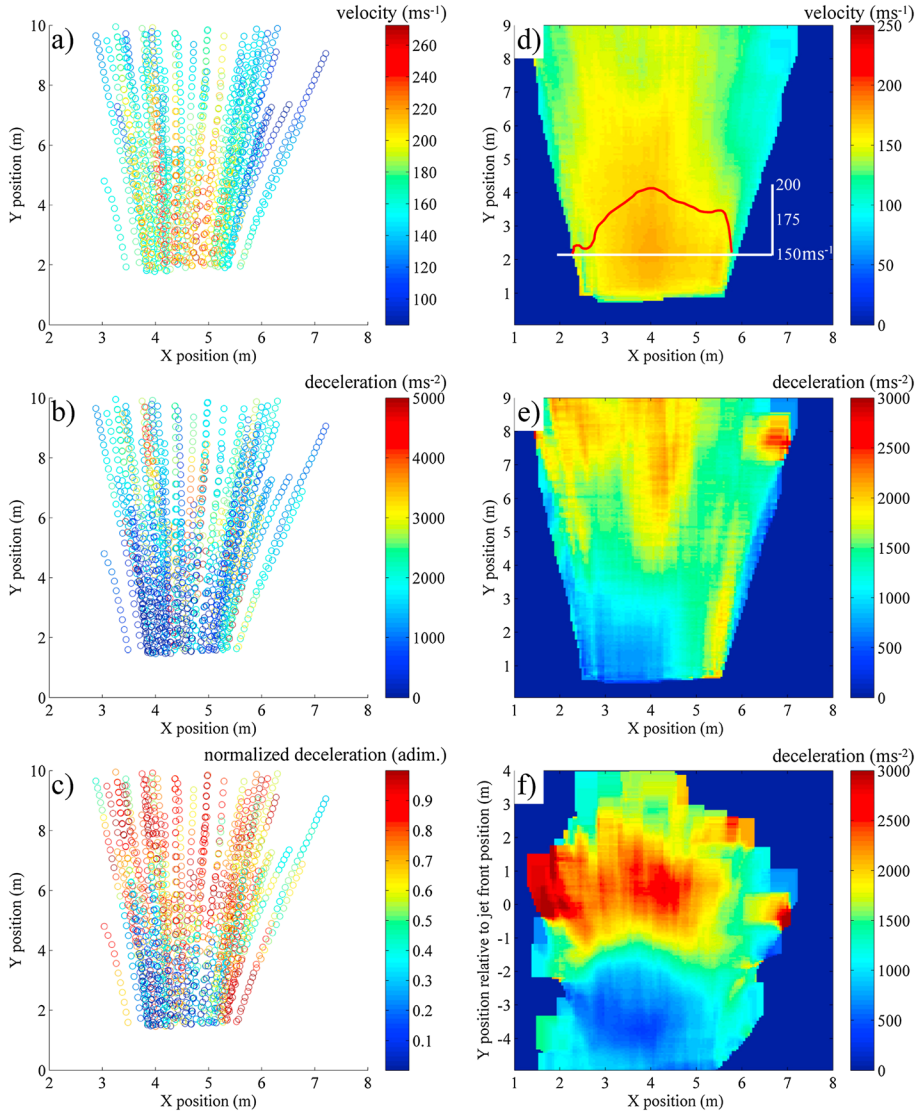

Figure 2. Example of the tracked trajectories of pyroclasts for one of the initial jets (at 13:32:34 GMT on 19 June 2009), with color bars referring to (a) vertical velocity, (b) deceleration, and (c) deceleration normalized between the minimum and maximum values of the data set, highlighting the locus of deceleration. (d) Velocity map of all tracked pyroclasts from the five studied explosions, obtained by averaging velocity on a moving window of 0.05 × 0.05 m. The red line is the velocity profile across the jet along the white, horizontal line. (e) Map of pyroclast deceleration. (f) Map of pyroclast deceleration relative to the position of the jet front. Note the localized deceleration in a narrow band close to the position of the jet front, underlain by a reduced deceleration area.

and the leading vortex is visible, obtaining 380 trajectories in the first 0.12 s of the explosions. A smaller subset of 114 trajectories, not included in the following analysis, covers later moments (from ~0.12 to 2 s), for a total of 494 pyroclasts and more than 10,000 track points. Tracked pyroclasts are 0.03–0.07 m in size (computed counting the number of pixels occupied over three to four frames). We also tracked the front of the leading vortex along several points using image difference frames (i.e., pixel by pixel subtraction and normalization of the grey level between one frame and the subsequent one), which allows a better visualization of the motion of the gas in and around the jet (Figure 1).

Each track point is defined by horizontal and vertical coordinates in the FOV and by a time. The vertical displacement and the interframe time interval provide the apparent vertical component of velocity on a plane perpendicular to the shooting direction. We divided this projected velocity by the sine of $90°-\alpha$ ($\alpha = 31°$, the camera tilt angle below horizontal) [*Taddeucci et al.*, 2012], effectively correcting the velocity

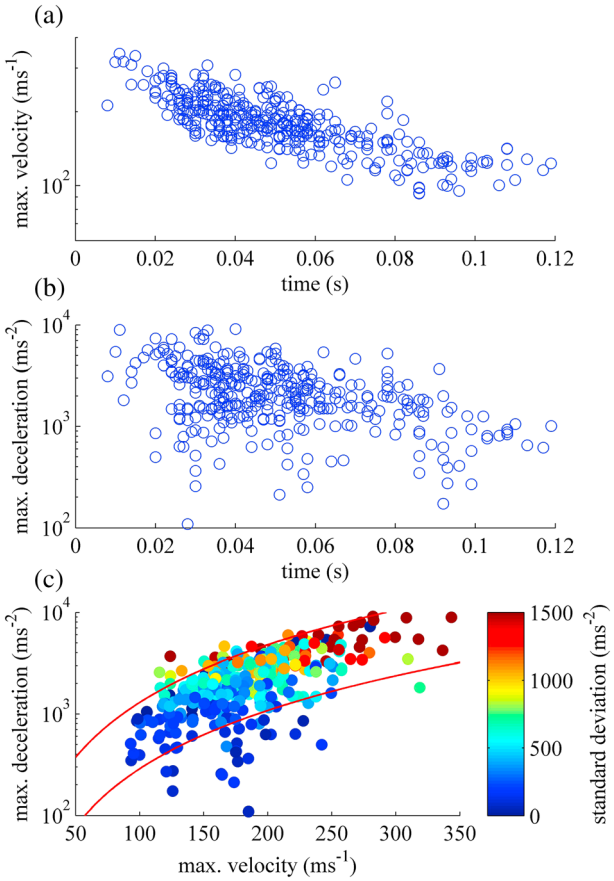

Figure 3. (a) Maximum velocity and (b) deceleration of pyroclasts as a function of their ejection time. (c) Maximum velocity versus maximum deceleration, color coded for the standard deviation of deceleration (computed over the whole trajectory). Higher standard deviations mirror larger deceleration gradients. The red lines represent the theoretical behavior (including gravity and drag) of pyroclasts with, e.g., 0.03 m diameter, 1200 kg m^{-3} density, and drag coefficient = 4.4 (upper line) and 1 (lower line) moving through still air at Stromboli ambient conditions.

of vertically ejected pyroclasts, which is mostly the case in our videos. The tracked pyroclasts may not have been homogeneously distributed throughout the jet but located preferentially on the jet side facing the high-speed camera. Although it is hard to quantify this bias, the relatively low pyroclast concentration in the studied jets (through which the background is still visible in the videos) leaves us confident that this effect did not significantly affect our results.

After smoothing the time-vertical velocity curve with the locally weighted least squared error method [e.g., *Cleveland*, 1979], we computed the vertical component of instantaneous acceleration as the first derivative of this velocity over time.

3. Pyroclast Deceleration

Within the FOV, pyroclast trajectories are relatively well collimated (±8° from the vertical) and straight to slightly curved. Pyroclast velocity (up to 350 m s^{-1}), within our limited size range, is independent of size and decreases over time (Figures 1 and 2). In contrast, the rise velocity of the five measured leading vortexes, ranging 53–141 m s^{-1}, remains approximately constant over the entire FOV (Figure 1). Within the first 0.12 s of the explosions, the mean velocity of the leading vortex (Vv) is proportional to the mean velocity of pyroclasts (Vp_{mean}) according to $Vv = 1.23Vp_{mean} - 103.48$ ($R^2 = 0.9055$).

Pyroclast velocity decreases over time at a relatively constant rate in 29.7% of the cases in the first 0.12 s of the explosion (56.5% of the cases in the later times of the same explosion, from 0.12 to 2 s). Conversely, 3.5% (4.3% from 0.12 to 2 s) of the pyroclasts travel, mostly along the jet central streamline, at a constant velocity over the

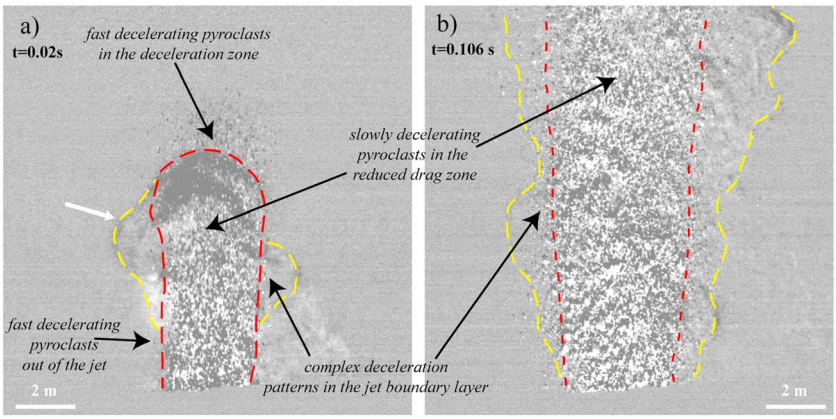

Figure 4. Difference images of the initial jet at (a) 0.020 s and (b) 0.106 s after the appearance of the first pyroclast. The red and yellow dashed lines enclose the sides of the jet and of eddies at its side, respectively. Pyroclasts decelerate abruptly across and ahead of the developing leading vortex ring (white arrow) (Figure 4a) or from the jet sides. Complex deceleration patterns develop when pyroclasts cross the shear layer and eddies present at the jet sides (Figure 4b). Over time, the gas-pyroclast coupling (or reduced drag) zone moves upward with the jet front and attenuates while jet velocity decreases and jet boundaries became more diffuse.

entire FOV. Trajectories beginning with a constant velocity and then dropping into deceleration represent up to 53.9% (and an addition 27.7% from 0.12 to 2 s). Finally, more complex deceleration patterns include multiple deceleration steps or even rare, short periods of pyroclast acceleration (from 12.9% to 11.4% of the whole measured pyroclasts). Decelerations in the order of 2×10^3 m s^{-2} are common, with peak values of more than 9×10^3 m s^{-2} (~10^3 times that of gravity).

3.1. Over Space

Combining the trajectory of all tracked pyroclasts, and averaging the velocity and acceleration values over a moving window of 5×5 cm, we obtain velocity and acceleration maps integrating the data from all five explosions. The distribution of pyroclast velocity within the jet is nonuniform, defining a broadly conical profile centered on the jet center streamline (Figure 2d). Pyroclasts decelerate in different parts of the jet, both at its sides and center, but, interestingly, the average deceleration is relatively low in the first few meters directly above the vent (Figure 2e). Observation of the videos and Figure 1 suggest that the interaction between the rising pyroclasts and the jet front, represented by the leading vortex, plays an important role in the pyroclast deceleration patterns. In order to uncover this role, in the last deceleration map (Figure 2f), for each explosion we normalized the vertical coordinate of all track points at any time by subtracting from the original coordinate the vertical coordinate of the respective jet front at the same time. It appears that pyroclast deceleration strongly focuses in a narrow (~2 m) band across the jet front, while below this band there is a zone where pyroclast deceleration is strongly attenuated.

3.2. Over Time

From each trajectory we extracted the maximum velocity and maximum deceleration experienced by the pyroclast, as well as the standard deviation of the deceleration along the entire trajectory. The standard deviation is well suited to measure changes in deceleration experienced by each pyroclast while traveling in the FOV and reveal the presence of complex deceleration patterns (see Figure 1d). The ejection velocity of pyroclasts decreases over time. Maximum deceleration decreases over time as well, but at a different (i.e., exponential) rate. It follows that pyroclast deceleration decreases nonlinearly with decreasing velocity (Figure 3). Also, the standard deviation of the deceleration decreases with decreasing velocity. This velocity-deceleration trend is similar to that of a drag-dominated system, in which deceleration increases with the square of velocity. The red lines in Figure 3 represent the velocity-deceleration relationship predicted according to classical aerodynamic theory [e.g., *Alatorre-Ibarguengoitia and Delgado-Granados*, 2006] for pyroclasts moving through still air at Stromboli ambient conditions and with a range of physical characteristics. For instance, the upper bound of the observed velocity-deceleration relationship can be approximated by pyroclasts 0.03 m in diameter, 1200 kg m^{-3} in density, and drag coefficient Cd = 4.4

(Figure 3, upper line), while a Cd = 1 (Figure 3, lower line), a value often used in literature, plots toward the lower bound. It appears that at any velocity, pyroclasts with lower standard deviation of the deceleration also experienced lower maximum deceleration.

4. Discussion

4.1. Sources of Deceleration

Gravity deceleration (9.8 m s^{-2}) plays a negligible role in our case, as pyroclasts decelerate at 10^2–10^4 m s^{-2}. Variable deceleration patterns could result from in-flight pyroclasts collisions [*Vanderkluysen et al.*, 2012]. However, the lack of sharp bends in the tracked trajectories and the observed systematic deceleration patterns rule out this hypothesis. In addition, not a single collision was observed while tracking, despite such collisions are clearly visible in other high-speed videos. Thus, we believe that the observed deceleration patterns mirror the dynamics of two-way coupling between gas and pyroclasts in initial volcanic jets.

The five initial jets we are dealing with correspond to individual ejection pulses [*Taddeucci et al.*, 2012, 2015; *Gaudin et al.*, 2014], characterized by a nonlinear decay of the ejection velocity over time and linked to the pressure and depth of the gas pocket driving the explosions. Decreasing ejection velocity is paralleled by decreasing deceleration, the two parameters being exponentially related in agreement with a drag-dominated system (Figure 3). However, in contrast to a simple drag-dominated system, for any given velocity we see a range of decelerations, larger ones being associated with larger standard deviations, i.e., steeper deceleration gradients. Larger decelerations (implying stronger drag force) can be expected for pyroclasts entering still, ambient air at higher velocities. This condition occurs both at the jet front, as pyroclasts overrun the leading vortex, and near the vent, when pyroclasts exit at an angle with respect to the jet center. In the former case, velocity is nearly constant while the pyroclast travels within the expanding gas in the jet; then velocity drops and deceleration increases suddenly as the pyroclast overruns the jet front (Figure 4). In the latter case, pyroclasts decelerate abruptly from the beginning. Smaller decelerations (i.e., smaller drag forces) are likely to occur inside the jet, where pyroclasts travel in close proximity to each other within the gas. In between these two end-members, there can be a variety of complex deceleration patterns, e.g., for pyroclasts traveling along the jet edges that experience velocity fluctuations at the jet boundary layer. These differences, together with a certain range of variability in pyroclast size, shape, and density, may explain the variable drag experienced by pyroclasts traveling at the same maximum velocity (Figure 3). Thus, it is not surprising that no simple drag force modeling solution exists for the tracked pyroclasts. These travel at a broad range of relative velocities with respect to the gas phase that changes in composition, temperature, and particle concentration, resulting in highly variable Reynolds, Mach, and Stokes numbers. We note that the upper bound of the velocity-deceleration trend in Figure 3c can be approximated only by imposing relatively high (>1) drag coefficients for realistic values of pyroclast size, density, and Reynolds number, in agreement with *de' Michieli Vitturi et al.* [2010].

4.2. Deceleration Zone and Reduced Drag Zone

The spatial pattern of pyroclast deceleration outlines, right above the vent, a region with reduced deceleration (Figure 2). Such a reduced drag zone has been included in several ballistic transport models [*Fagents and Wilson*, 1993; *Mastin*, 2001], the latter author warning that "The degree to which such drag is reduced and the distance over which drag is less than that in ambient air are not well constrained." *Fagents and Wilson* [1993] modeled the reduced drag zone in Vulcanian eruptions as a radially symmetric, hemispherical area above the vent, where pyroclasts first accelerate irrespectively of size and/or density and then decelerate exponentially over time together with the surrounding, expanding atmosphere. Our results show that the drag reduction zone can be more collimated, as related with the presence of a jet, and that drag increase may be more abrupt than exponential. Based on our results, if the largest and highest velocity blocks are ejected at the very beginning of the explosion, the radial extent of the reduced drag zone might be on the order of the vent diameter.

We seldom observe pyroclast acceleration, which instead occurs in the conduit, and jet dynamics, rather than radial expansion, control the two-way coupling. This control is evident in image difference still frames of the initial jets (Figure 4): at 0.02 s from its appearance, the jet features an incipient leading vortex crossed by centimeter-sized pyroclasts, and sharp boundaries. At 0.106 s, the jet front is already out of the FOV, the jet is larger and has smoother boundaries (i.e., larger shear zone).

Pyroclast deceleration occurs at the jet sides and, mostly, in a narrow band (apparently 2 m wide, but possibly even less, considering our 2-D view), or deceleration zone, across the jet front (Figure 2), with an average deceleration in the order of 3000 m s^{-2}. Upstream the deceleration zone there is a reduced drag zone where the average deceleration is significantly lower. Both zones move upward with the jet front and are expected to attenuate away from the vent as a result of the decreasing pyroclast velocity and concentration in the jet with height and time. We infer the deceleration zone to correspond with the zone where pyroclasts, driven by inertia, overrun the slower-rising leading vortex ring (Figure 4). These pyroclasts suddenly enter the still air present ahead of the zone affected by the motion of the vortex and decelerate by drag, in turn moving air upward and feeding the vortex. The reduced drag zone corresponds to the area within the jet where pyroclasts are partly or wholly coupled with the gas. We observed the formation of a leading vortex ring pierced by rising pyroclasts also during Vulcanian-style eruptions at Sakurajima volcano (southern Japan), suggesting that, despite differences in eruption magnitude, intensity, and style, the two-way coupling dynamics documented here for Strombolian explosions may also be relevant for other transient eruption styles.

5. Perspectives

Pyroclast deceleration is dominated by drag force and controlled by jet dynamics. It focuses in a narrow zone at the front of the eruption jet, reaching surprisingly high values, while it is much reduced within the jet, where pyroclasts travel coupled with the gas.

The relatively slow and large leading vortex ring that characterize almost all eruption plumes, not only at Stromboli, can be tracked using conventional (either visible or thermal) monitoring cameras [*Harris et al*., 2012], while fast-moving pyroclasts can be tracked only by a high-speed camera equipped with zoom lenses, unsuitable for continuous volcano monitoring. The relationship we found between the rise velocity of the vortex and the average velocity of pyroclasts could be used to routinely infer averaged pyroclast exit velocity at monitored volcanoes.

The findings delineated above strongly impact the modeling of pyroclast ejection, trajectory, and landing distance. Such modeling, in turn, is widely used for developing hazard maps at active volcanoes, in calculating the energetics of past eruptions from their ejecta, and in inferring the paleodensity of extraterrestrial atmospheres [*Manga et al*., 2012]. The values obtained here for the extent of the reduced drag zone and the degree of drag reduction within it are, to the best of our knowledge, the first quantitative parameterization of pyroclast deceleration during Strombolian explosions, and the general dynamics outlined in this work could potentially apply to larger, jet-forming, and highly transient eruptive styles like Hawaiian fountaining, Vulcanian, and Violent Strombolian ones. Our results point toward a more comprehensive modeling of ballistic trajectories of volcanic bombs, and future models should rely on the observed time and space trends in pyroclast deceleration patterns.

In this note, we focused on the effect of drag in decelerating lapilli- to bomb-sized pyroclasts. Drag, on the other hand, is also an effective way to transfer momentum from relatively coarse pyroclasts to the surrounding gas phase and the ash particles coupled with it. The strong deceleration of pyroclasts at the jet front continuously feed momentum to the leading vortex ring which, in turn, is the main motor of air entrainment into the jet and the buoyant rise of the ash plume above the jet. Thus, it is quite likely that the two-way coupling dynamics that we described and quantified for relatively coarse grained pyroclasts are also relevant for the atmospheric dispersal of finer material.

Acknowledgments

Data supporting this article are provided at INGV Roma, Department of Seismology and Tectonophysics, HP-HT Lab, data set Stromboli_190609. Funding was provided by INGV-DPC "V2" and "Paroxysm" and FIRB-MIUR "Research and Development of New Technologies for Protection and Defense of Territory from Natural Risks." D. Andronico, U. Kueppers, S. Mueller, and Zazà supported field activities. An anonymous reviewer and Loyc Vanderkluysen provided precious corrections and suggestions.

The Editor thanks Larry Mastin and Loÿc Vanderkluysen for their assistance in evaluating this paper.

References

Abramoff, M. D., P. J. Magelhaes, and S. J. Ram (2004), Image processing with ImageJ, *Biophotonics Int.*, *11*, 36–42.

Alatorre-Ibarguengoitia, M. A., and H. Delgado-Granados (2006), Experimental determination of drag coefficient for volcanic materials: Calibration and application of a model to Popocatépetl volcano (Mexico) ballistic projectiles, *Geophys. Res. Lett.*, *33*, L11302, doi:10.1029/2006GL026195.

Alatorre-Ibarguengoitia, M. A., H. Delgado-Granados, and D. B. Dingwell (2012), Hazard map for volcanic ballistic impacts at Popocatépetl volcano (Mexico), *Bull. Volcanol.*, *74*, 2155–2169, doi:10.1007/s00445-012-0657-2.

Bombrun, M., A. Harris, L. Gurioli, J. Battaglia, and V. Barra (2015), Anatomy of a Strombolian eruption: Inferences from particle data recorded with thermal video, *J. Geophys. Res. Solid Earth*, *120*, 2367–2387, doi:10.1002/2014JB011556.

Cleveland, W. S. (1979), Robust locally weighted regression and smoothing scatterplots, *J. Am. Stat. Assoc.*, *74*, 829–836.

de' Michieli Vitturi, M., A. Neri, T. Esposti Ongaro, S. Lo Savio, and E. Boschi (2010), Lagrangian modeling of large volcanic particles: Application to Vulcanian explosions, *J. Geophys. Res.*, *115*, B08206, doi:10.1029/2009JB007111.

Fagents, S. A., and L. Wilson (1993), Explosive volcanic eruptions—VII. The ranges of pyroclasts ejected in transient volcanic explosions, *Geophys. J. Int.*, *113*(2), 359–370, doi:10.1111/j.1365-246X.1993.tb00892.x.

Gaudin, D., J. Taddeucci, P. Scarlato, M. Moroni, C. Freda, M. Gaeta, and D. M. Palladino (2014), Pyroclast Tracking Velocimetry illuminates bomb ejection and explosion dynamics at Stromboli (Italy) and Yasur (Vanuatu) volcanoes, *J. Geophys. Res. Solid Earth*, *119*, 5384–5397, doi:10.1002/2014JB011096.

Global Volcanism Program (2015), Report on Ontakesan (Japan), in *Bulletin of the Global Volcanism Network*, edited by R. Wunderman, vol. 40, Smithsonian Institution, doi:10.5479/si.GVP.BGVN201503-283040.

Harris, A., M. Ripepe, and E. A. Hughes (2012), Detailed analysis of particle launch velocities, size distributions and gas densities during normal explosions at Stromboli, *J. Volcanol. Geotherm. Res.*, *231–232*, 109–131, doi:10.1016/j.jvolgeores.2012.02.012.

Kieffer, S. W., and B. Sturtevant (1984), Laboratory studies of volcanic jets, *J. Geophys. Res.*, *89*, 8253–8268, doi:10.1029/JB089iB10p08253.

Manga, M., A. Patel, J. Dufek, and E. S. Kite (2012), Wet surface and dense atmosphere on early Mars suggested by the bomb sag at Home Plate, Mars, *Geophys. Res. Lett.*, *39*, L01202, doi:10.1029/2011GL050192.

Mastin, L. G. (2001), A simple calculator of ballistic trajectories for blocks ejected during volcanic eruptions, *U.S. Geol. Surv. Open File Rep., 01–45*, p. 26.

Patrick, M. R. (2007), Dynamics of Strombolian ash plumes from thermal video: Motion, morphology, and air entrainment, *J. Geophys. Res.*, *112*, B06202, doi:10.1029/2006JB004387.

Taddeucci, J., M. A. Alatorre-Ibargüengoitia, M. Moroni, L. Tornetta, A. Capponi, P. Scarlato, D. B. Dingwell, and D. De Rita (2012), Physical parameterization of Strombolian eruptions via experimentally-validated modeling of high-speed observations, *Geophys. Res. Lett.*, *39*, L16306, doi:10.1029/2012GL052772.

Taddeucci, J., M. Edmonds, B. Houghton, M. R. James, and S. Vergniolle (2015), Hawaiian and Strombolian eruptions, in *The Encyclopedia of Volcanoes*, 2nd ed., edited by H. Sigurdsson et al., pp. 485–503, Academic Press, London.

Vanderkluysen, L., A. Harris, K. Kelfoun, C. Bonadonna, and M. Ripepe (2012), Bombs behaving badly: Unexpected trajectories and cooling of volcanic projectiles, *Bull. Volcanol.*, *74*, 1849–1858, doi:10.1007/s00445-012-0635-8.

Wilson, L. (1972), Explosive volcanic eruptions—II. The atmospheric trajectories of pyroclasts, *Geophys. J. R. Astron. Soc.*, *30*, 381–392.